# Radiosynthesis and biological evaluation of a novel enoyl-ACP reductase inhibitor for Staphylococcus aureus

**ARTICLE** *in* EUROPEAN JOURNAL OF MEDICINAL CHEMISTRY · SEPTEMBER 2014

Impact Factor: 3.45 · DOI: 10.1016/j.ejmech.2014.09.008 · Source: PubMed

European Journal of Medicinal Chemistry xxx (2014) 1–8

Contents lists available at ScienceDirect

European Journal of Medicinal Chemistry

journal homepage: http://www.elsevier.com/locate/ejmech

Original article

# Radiosynthesis and biological evaluation of a novel enoyl-ACP reductase inhibitor for *Staphylococcus aureus*

Hui Wang [a, 1], Yang Lu [a, 1], Li Liu [a, 2], Sung Won Kim [b, 3], Jacob M. Hooker [b, 4], Joanna S. Fowler [b], Peter J. Tonge [a, *]

[a] Institute of Chemical Biology & Drug Discovery, Department of Chemistry, Stony Brook University, Stony Brook, NY 11794, USA
[b] Biosciences Department, Brookhaven National Laboratory, Upton, NY 11973, USA

ARTICLE INFO

*Article history:*
Received 11 June 2014
Received in revised form
27 August 2014
Accepted 3 September 2014
Available online xxx

*Keywords:*
*Staph aureus* enoyl-ACP reductase (saFabI)
Pharmacokinetics
Pharmacodynamics
Positron emission tomography
Antibacterial efficacy

ABSTRACT

The pharmacokinetics (PK) and pharmacodynamics (PD) of PT119, a potent *Staphylococcus aureus* enoyl-ACP reductase (saFabI) inhibitor with a $K_i$ value of 0.01 nM and a residence time of 750 min on the enzyme target, has been evaluated in mice. PT119 was found to have promising antibacterial activity in two different *S. aureus* infection models: it caused a 3 log reduction in the CFU's in a mouse thigh muscle infection model and increased the survival rate from 0% to 50% in a mouse systemic infection model. PT119 was then radiolabeled with carbon-11 to evaluate its biodistribution and PK in both healthy and *S. aureus* infected mice using positron emission tomography (PET). The biodistribution of [$^{11}$C]PT119 and/or its labeled metabolites did not differ significantly between the healthy group and the infected group, and PT119 was found to distribute equally between serum and tissue during the ~1 h of analysis permitted by the carbon-11 half life. This approach provides important data for PK/PD modeling and is the first step in identifying radiotracers that can non-invasively image bacterial infection *in vivo*.



## 1. Introduction

Target tissue pharmacokinetics (PK), the link between plasma PK and drug effects [1], has emerged as an important facet in drug discovery and development. Although plasma PK is often used as a surrogate for tissue PK, the equilibrium between plasma and target tissue cannot always be taken for granted; drug levels in target tissues are often substantially different from the corresponding plasma levels [1,2]. In the case of antibiotic compounds, suboptimal tissue drug concentrations resulting from estimates based on plasma PK, can not only lead to therapeutic failure but also trigger bacterial resistance [3]. Thus, current Food and Drug Administration (FDA) guidelines require tissue drug distribution studies at infected and uninfected sites [2]. Positron emission tomography (PET), which images drugs and other molecules labeled with positron-emitting isotopes (primarily nitrogen, oxygen, carbon, and fluorine), has been applied in creative ways to study drug action directly in humans and laboratory animals [4]. In addition, the methodology developed for studying drug distribution in laboratory animals using PET can be readily translated to humans [5].

*Staphylococcus aureus* is a highly infectious pathogen that is carried by 30% of healthy people, usually in the anterior nasal cavities. It is the most common causative agents of nosocomial infections and is readily transferred to immunocompromised patients and causes post-surgical wound infections [6-8]. *S. aureus* is able to acquire resistance to antibiotics rapidly, and methicillin-resistant strains (MRSA) emerged only one year after the introduction of this antibiotic in 1959 [9]. MRSA infection has spread in the past few decades and is treated by vancomycin, the “drug of last resort” [10]. Unfortunately, vancomycin-resistant strains (VRSA) were isolated in June 2002 [11] and there is therefore an urgent need to continuously discover new drugs to combat *S. aureus*.

The type II fatty acid biosynthesis pathway (Fig. 1a), which is usually found in plants and bacteria, is responsible for the *de novo* production of lipids for incorporation into the bacterial cell membrane [12]. The final step in fatty acid elongation is catalyzed by the enoyl-ACP reductase enzyme, which has emerged as an attractive drug target in those pathogens that contain the FabI homologue [13]. Isoniazid (Fig. 1b), a front-line tuberculosis prodrug, is known

* Corresponding author.
*E-mail address:* peter.tonge@stonybrook.edu (P.J. Tonge).
[1] These two authors contributed equally.
[2] Present address: Center for Biotechnology, Stony Brook, NY 11794, USA.
[3] Present address: Laboratory of Neuroimaging, National Institute of Alcohol Abuse and Alcoholism, Bethesda, MD 20892, USA.
[4] Present address: Martinos Center for Biomedical Imaging, Massachusetts General Hospital Radiology, Harvard Medical School, Charlestown, MA 02129, USA.

http://dx.doi.org/10.1016/j.ejmech.2014.09.008
0223-5234/

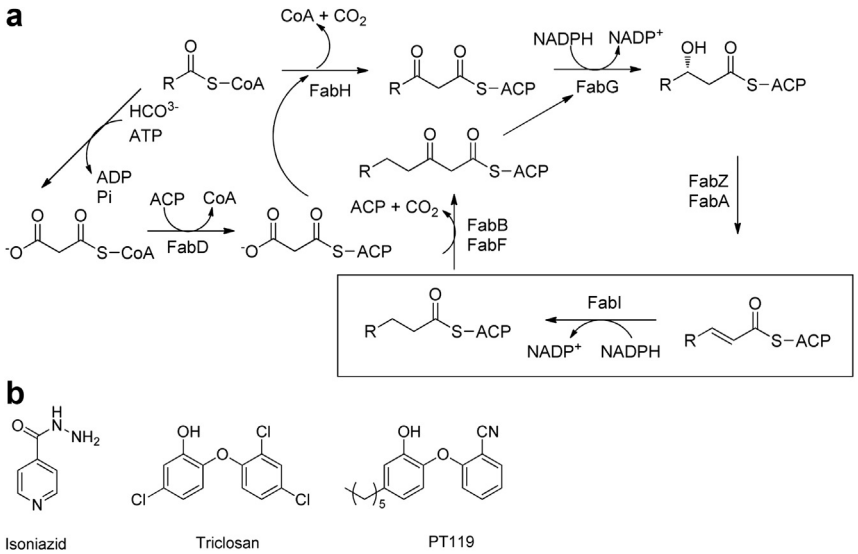


**Fig. 1.** a. The fatty acid biosynthesis pathway in *S. aureus*. b. Examples of FabI inhibitors.

to target InhA, the FabI homologue in *Mycobacterium tuberculosis* [14] while triclosan (TCL; Fig. 1b), a diphenyl ether inhibitor of the *S. aureus* FabI (saFabI), is recommended as a topical antiseptic to reduce MRSA skin colonization [15]. Furthermore, three separate saFabI inhibitors are currently in clinical trials for treating infection caused by drug-resistant *S. aureus* [16–18].

We recently reported a series of 20 diphenyl ether saFabI inhibitors in which explored the SAR for long residence time inhibition of saFabI [19]. Residence time is defined as the reciprocal of the enzyme-inhibitor dissociation rate constant, and is a promising early stage indicator of *in vivo* drug efficacy [20]. Our most potent compound PT119 (Fig. 1b; $K_i = 0.01$ nM) has a residence time of 750 min because of its favorable interactions with the enzyme [19]. It also shows a promising Minimum Inhibitory Concentration (MIC) value of 0.5 μg/mL (unpublished data).

Herein, we report the radiolabeling of our lead compound PT119 with carbon-11 (half life: 20.4 min) to evaluate its biodistribution in both healthy and *S. aureus* infected mice. We also report the pharmacokinetics of PT119 by both intravenous and subcutaneous routes. Furthermore, we report the *in vivo* efficacy of PT119 in two different infection models.

## 2. Materials and methods

### 2.1. General

All chemicals used in the study were purchased from commercial vendors and were used without further purification except where stated.

[$^{11}$C]HCN was generated from [$^{11}$C]$CO_2$ using a custom-built automated synthesis unit [21]. Briefly, [$^{11}$C]$CO_2$ was obtained from proton bombardment of a $N_2/O_2$ target ($^{14}$N(p,α)$^{11}$C) using an EBCO TR 19 cyclotron (Advanced Cyclotron System Inc., Richmond, Canada) and trapped on molecular sieves with an embedded Ni catalyst. The trapped [$^{11}$C]$CO_2$ was heated to 350 °C with $H_2$ on nickel catalyst to produce [$^{11}$C]$CH_4$. Subsequent reaction of [$^{11}$C]$CH_4$ and $NH_3$ was catalyzed by platinum at 950 °C and produced [$^{11}$C]HCN, which was carried by a stream of argon into our shielded hot cell for radiosynthesis.

Analytical and preparative high performance liquid chromatography (HPLC) were performed using a Knauer HPLC system (Sonntek Inc., Woodcliff Lake, NJ, USA) equipped with a model K-5000 pump, a Rheodyne 7125 injector, a model 87 variable wavelength monitor, and a NaI radioactivity detector. Specific activity was determined by measuring the radioactivity and the mass; the latter was derived from a standard curve (UV absorbance at 254 nm by peak area) after HPLC injection of different quantities of the authentic reference compound. The purities of the intermediate and final products were >95%. The specific solvent gradients used for each compound are given below.

### 2.2. Chemistry – synthesis of reference PT119 and precursor for labelling

The synthesis of the reference compound PT119 has been described previously [22]. Precursor **7** was synthesized by multistep organic synthesis (Scheme 1). First, vanillin was protected with a benzyl group and coupled with a hexyl chain using a Wittig reaction to form compound **2**, after which hydrogenation was used to generate compound **3**. Compound **4** was synthesized by nucleophilic aromatic substitution of **3** with 1-fluoro-2-nitrobenzene, and was converted to compound **5** by reduction with $H_2$ catalyzed by palladium on charcoal. Compound **6** was prepared from **5** by utilizing the Sandmeyer reaction, which proceeded through a diazonium salt intermediate prior to iodide anion attack. The deprotection was carried out with tribromoborane in dichloromethane to form **7** [22].

### 2.3. Radiosynthesis of [$^{11}$C]-PT119

The synthesis of [$^{11}$C]PT119 was performed using the iodo-precursor **7**. The precursor **7** (1.0 mg), $K_{222}$(0.2 mg) and tetrakis (triphenylphosphine) palladium (0) (2.0 mg) was placed in a vial with 0.2 ml DMSO and heated slightly until all the solid dissolved. This solution was then added to [$^{11}$C]HCN that had been purged and trapped in 0.15 ml DMSO. The reaction solution was sealed in a reaction vial and heated at 135 °C for 5 min in an oil bath. The reaction was quenched by the addition of 1 ml water and the mixture was filtered through celite prior to injection onto a reverse phase

Please cite this article in press as: H. Wang, et al., Radiosynthesis and biological evaluation of a novel enoyl-ACP reductase inhibitor for *Staphylococcus aureus*, European Journal of Medicinal Chemistry (2014), http://dx.doi.org/10.1016/j.ejmech.2014.09.008

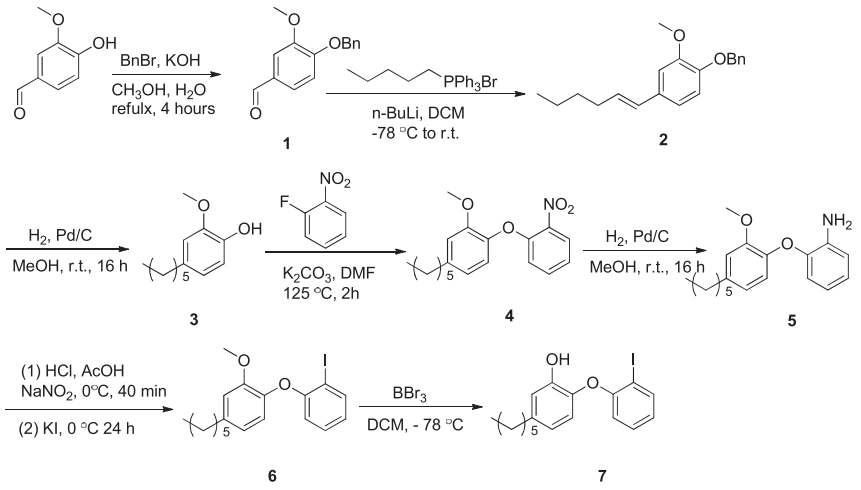


**Scheme 1.**

PFP semi-preparative column (Phenomenex, Luna PFP 250 × 10, 5 μm), at a 5 mL/min flow rate with a mobile phase consisting of 70% MeCN/30% aqueous ammonium formate (0.1 M) using UV (254 nm) and radiodetection. The product was collected at the expected retention time (10 min) based on a standard and the solvent was removed by rotary evaporation. After dilution with 1 mL sterile alcohol plus 4 mL saline, the solution was filtered through an Acrodisc 13-mm syringe filter with 0.2 μm Supor membrane into a sterile vial for delivery. Radiochemical purity was determined by reversed-phase analytical HPLC using a Phenomenex, Luna PFP, 250 × 4.6, 5 μm column operated at 1.0 mL/min flow rate using a mobile phase of 70% MeCN/30% $H_2O$ monitored by UV (254 nm) and radiodetection, with 10 min retention time. Subsequently, purity was verified using TLC (5% EA/95% HE, $R_f = 0.4$) by co-spotting the labeled product with a standard.

### 2.4. Infection models

All animals used in this study were maintained in accordance with the American Association for Accreditation of Laboratory Animal Care criteria. The experimental protocol was approved by the Institutional Animal Care and Use Committees (IACUC) at Stony Brook University and Brookhaven National Laboratory.

Six-week old, specific pathogen free, male Swiss Webster mice weighing 28–32 g were purchased from Taconic and housed in the Division of Laboratory Animal Resources (DLAR) at Stony Brook University under Biosafety Level − 2 (BSL − 2) conditions. All mice were given *ad libitum* access to food and water throughout the entire study. Prior to infection, mice were rendered neutropenic by treatment with cyclophosphamide on day -4 (150 mg/kg) and day -1 (100 mg/kg) via intraperitoneal injection (ip).

Bacterial stocks were freshly prepared before inoculation. In general, MRSA strain BAA1762 was cultured in Mueller Hinton broth at 37 °C to mid log phase ($OD_{600} = 0.45$, $2 \times 10^8$ cells/ml). Bacterial cells were harvested by centrifugation (11,000 rpm, 3 min) and washed with sterilized brain heart infusion (BHI) broth. Final inoculums were generated by diluting bacteria to the desired concentrations in BHI broth. Two infection models were used in this study, a systemic infection model and a thigh muscle infection model. To induce systemic infection, mice were injected with $2 \times 10^7$ bacterial cells ($2 \times 10^8$ cells/mL inoculum, 100 μL) intraperitoneally. Thigh infections were established by injecting $5 \times 10^5$ bacterial cells ($10^7$ cells/mL inoculum, 50 μL) into the left thigh muscles of mice.

### 2.5. In vivo antibacterial efficacy of PT119

In order to determine *in vivo* efficacy, PT119 was formulated in a mixed solvent consisting ethanol/PEG-400/saline (40/20/40). In the systemic infection study, PT119 (100 mg/kg) was given by subcutaneous (sc) injection on day 0 (1 h post infection), day 1 and day 2 with a 24 h administration interval. The same dose of PT119 was administered each time. A group of infected mice treated with vehicle was used as a negative control whereas another group of healthy mice treated with vehicle was used as positive control. Survival was assessed twice a day after infection for 7 days in total and dead animals were removed as soon as they died. Survivors of the study were euthanized by $CO_2$ inhalation as recommended by the American Veterinary Medical Association (AVMA) guidelines on euthanasia. In the thigh muscle infection model, a single dose of PT119 (15, 40, 100 mg/kg) was given sc 1 h post infection. A group of infected mice treated with vehicle was used as negative control. All mice were euthanized by $CO_2$ inhalation 24 h post infection. Muscle tissue from the infected thighs was collected and homogenized in 1 mL of saline. Bacterial load was determined by counting colony forming unit (CFU) of serial dilutions on MH II-sheep blood agar plates.

### 2.6. Pharmacokinetics of PT119

The pharmacokinetics (PK) of PT119 was conducted in healthy Swiss Webster mice. Two administration routes, iv (10 mg/kg) and sc (40 mg/kg), were studied. After a single drug administration, blood samples were collected at 5 min, 15 min, 30 min, 1 h, 2 h, 4 h, 7 h and 24 h ($n = 3$). Each mouse was bled at two consecutive time points via retro − orbital bleeding and cardiac puncture, respectively, and ethylenediaminetetraacetic acid (EDTA) was used as the anticoagulant. Whole blood samples were centrifuged, and the plasma that resulted was treated with acetonitrile to precipitate the plasma proteins. After an additional centrifugation step, the supernatant was collected for LC-MS/MS analysis. The plasma concentration of PT119 from each administration route was calculated and analyzed using PK analysis software WinNonlin (NCA model). The bioavailability of sc administration was determined after dosing normalization.

### 2.7. Biodistribution of [$^{11}$C]-PT119

The *in vivo* biodistribution of [$^{11}$C]PT119 was determined in healthy mice and in both systemic infection and thigh infection

Please cite this article in press as: H. Wang, et al., Radiosynthesis and biological evaluation of a novel enoyl-ACP reductase inhibitor for *Staphylococcus aureus*, European Journal of Medicinal Chemistry (2014), http://dx.doi.org/10.1016/j.ejmech.2014.09.008

models. In brief, mice were anesthetized using isoflurane and stabilized in a mouse restrainer. Approximately 3.7 MBq of [$^{11}$C]PT119 in 50–200 μl ethanol/saline (1/3. v/v) was administered using the lateral tail vein. Treated mice were returned to their home cages, allowed to recover from anesthesia and were free to move during the uptake period. Mice were euthanized by cervical dislocation at different time points. In the systemic infection group, infected mice as well as healthy control mice were sacrificed at 20 min, 40 min and 60 min. The carcasses were dissected immediately and organs of interest (spleen, lung, liver and kidney) were harvested. Blood samples were collected by cardiac puncture. Tissue or blood samples were transferred into glass vials, weighed and counted using a well counter (Picker, Cleveland, OH). In the thigh infection group, infected mice and healthy control mice were euthanized at 15 min, 30 min, 45 min and 60 min. Muscle tissue from both thighs, as well as blood, were collected, weighed and counted. Radioactivity values are given as the percentage of total injection dose/g (%ID/g) and are expressed as the mean ± standard deviation (SD, $n = 3$).

## 3. Results

### 3.1. Radiosynthesis of [$^{11}$C]PT119

The radiosynthesis of [$^{11}$C]PT119 was accomplished by a one-step tetrakis (triphenylphoshpine) palladium (0) catalyzed cyanation (Scheme 2). This method was adapted from the previously reported radiolabeling of an aromatic ring with [$^{11}$C]HCN [23], and involved reaction with [$^{11}$C]HCN in DMSO for 5 min at 135 °C. The reaction mixture was subsequently purified by HPLC and fractions from HPLC were concentrated *in vacuo* to generate the dry product. Analytical HPLC and TLC demonstrated that the product was over 98% radiochemically pure with a specific activity of 18.5–29.6 GBq/μmol at the end of cyclotron bombardment (EOB). The final product was formed with an average 30%–50% decay-corrected yield in a total synthesis time of 50 min.

### 3.2. Biodistribution of [$^{11}$C]PT119 in thigh infected mice

In the *S. aureus* thigh infection model, the distribution patterns of [$^{11}$C]PT119 in the infected thigh, healthy thigh and blood were found to be similar (Fig. 2 and Table 1). There was no significant difference between infected thigh and healthy thigh, which suggests that *S. aureus* infection does not change the biodistribution of PT119. The distribution of [$^{11}$C]PT119 between the thighs and serum was also similar, indicating rapid equilibriation of PT119 between these two compartments.

### 3.3. Biodistribution of [$^{11}$C]PT119 in systemic infected and healthy mice

Peripheral organ drug distribution was determined in healthy mice and those with systemic *S. aureus* infection (Fig. 3 and Table 2). Again, no significant difference in drug concentrations was observed between infected tissues and healthy tissues. For all tissues measured, the highest concentration of drug was measured at 20 min after injection and decreased at later times.

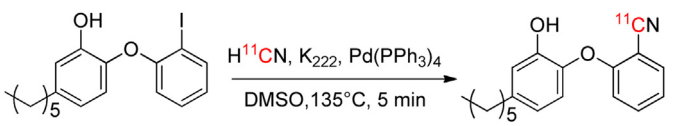


**Scheme 2.**

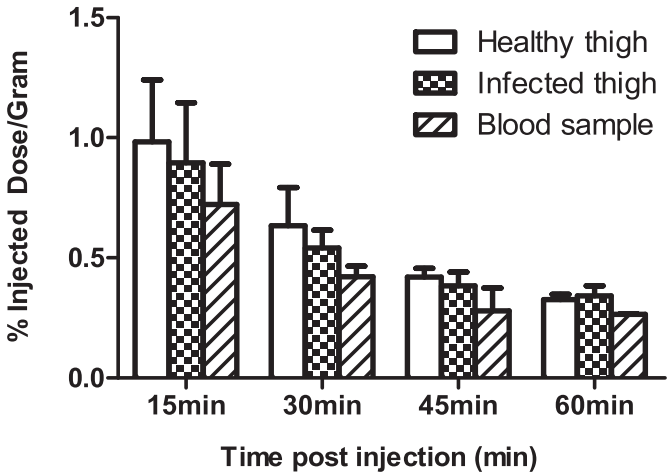


**Fig. 2.** Biodistribution of [$^{11}$C]PT119 in the *S. aureus* thigh infection model. Biodistribution of [$^{11}$C]PT119 in *S. aureus* infected thigh, healthy thigh and blood samples at 15, 30, 45 and 60 min after injection. The data are expressed as % injected dose/gram. Each value is the mean ± SD for three animals.

**Table 1**
Biodistribution in the thigh infection model.

| | Healthy thigh | Infected thigh | Blood |
|---|---|---|---|
| 15 min | 0.98 ± 0.21 | 0.89 ± 0.20 | 0.72 ± 0.13 |
| 30 min | 0.63 ± 0.13 | 0.54 ± 0.06 | 0.42 ± 0.04 |
| 45 min | 0.42 ± 0.03 | 0.38 ± 0.05 | 0.28 ± 0.07 |
| 60 min | 0.33 ± 0.02 | 0.34 ± 0.03 | 0.26 ± 0.01 |

Values given are [%ID/cc].

### 3.4. PT119 has efficacy in the S. aureus infected mice

The efficacy of PT119 was evaluated in both the *S. aureus* thigh muscle infection model and the systemic infection model. In the thigh infection model, a single dose of PT119 was delivered sc 1 h post infection. Then the muscle from the infected thigh was collected to enumerate bacterial load 24 h post infection. Untreated mice generally displayed 9 $\log_{10}$ CFU in infected thigh 24 h post infection. PT119 significantly reduced bacterial growth to 7 $\log_{10}$ CFU (40 mg/kg; Fig. 4) and 6 $\log_{10}$ CFU (100 mg/kg; Fig. 4). In the *S. aureus* systemic model, animals in the infection model were treated with PT119 for three consecutive days, starting from the day of infection and then monitored for four additional days. In general, our experiments showed that all treated animals survived longer than untreated control animals, indicating that PT119 has antibacterial activity and is able to reduce the bacterial load. Untreated control mice had 0% survival rate with a median survival of 1 day, whereas treatment with 100 mg/kg PT119 delivered sc resulted in a 50% median survival.

### 3.5. Pharmacokinetics and subcutaneous bioavailability of PT119

The pharmacokinetic parameters that were determined included AUC, $C_{max}$, $T_{max}$, F (bioavailability) and $t_{1/2}$ for PT119 following dosing at 10 mg/kg iv and 40 mg/kg sc (Fig. 5 and Table 3). The AUC of PT119, which evaluates drug exposure, was 0.64 or 1.77 h*μg/mL when delivered iv at 10 mg/kg or sc 40 mg/kg, respectively. Delivery of PT119 at 10 mg/kg iv resulted in a $C_{max}$ value of 0.84 μg/mL with a $T_{max}$ of 0.08 h, whereas a 40 mg/kg dose delivered sc yielded a $C_{max}$ value of 0.28 μg/mL with a $T_{max}$ of 4 h. The bioavailability (F) of PT119 was assessed to determine the fraction of the dose reaching the systemic circulation after

Please cite this article in press as: H. Wang, et al., Radiosynthesis and biological evaluation of a novel enoyl-ACP reductase inhibitor for *Staphylococcus aureus*, European Journal of Medicinal Chemistry (2014), http://dx.doi.org/10.1016/j.ejmech.2014.09.008

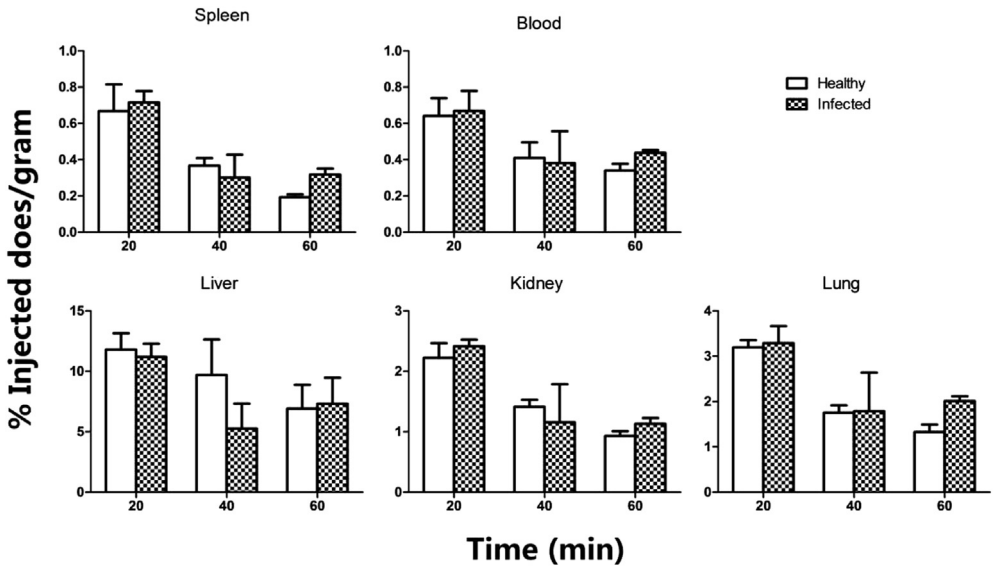


**Fig. 3.** Biodistribution of [$^{11}$C]PT119 in the *S. aureus* systemic infection model. Biodistribution of [$^{11}$C]PT119 in healthy mice and *S. aureus* systemic infected mice at 20, 40 and 60 min after injection. The data are expressed as % injected dose/gram. Each value is the mean ± SD for three animals.

administration. PT119 delivered sc at 40 mg/kg had an F value of 69% (Table 3).

## 4. Discussion

The type II fatty acid biosynthesis pathway (FASII) is a promising target for novel antibacterial drug discovery [13,24] and, using structure-based design, we have developed a series of diphenyl ethers that are potent FASII FabI enzyme inhibitors. Importantly, the activity of the FabI inhibitors against several bacterial pathogens confirms that this enzyme is a sensitive target for the development of broad-spectrum chemotherapeutics [20,25,26], and led to the discovery of PT119. Here, we extended our studies on PT119 and developed a radiolabelling method using the PET isotope carbon-11 to determine the biodistribution and pharmacokinetics parameters of this compound. The use of carbon-11 labeling enables the biodistribution of PT119 to be determined without altering the structure of the parent compound. However, the short half-life of carbon-11 (20.4 min) not only makes labelling challenging, but also limits the time window for monitoring drug distribution after administration. In this study, radiosynthesis and formulation of [$^{11}$C]PT119 has been accomplished in 1 h using [$^{11}$C]HCN, enabling at least one additional hour for determining the biodistribution of this compound.

The use of PET imaging to study pharmacokinetics has many advantages over other conventional techniques [4,27]. Although in this study drug concentrations in tissues are determined by radioactivity measured in excised tissues (*ex vivo*), the method can easily be translated to larger species including human subjects, where multiple measurements in the same subject at different times and in a variety of physiologic or pathologic states would be feasible. Another major benefit of PET imaging is that it is a quantitative measurement. Besides the translational potential and quantitative potential, PET can also be used to determine target engagement in human subjects if specific binding of a radiotracer is observed. It is important to determine target engagement because the pharmacological validation of drug action requires verification that chemical probes engage their intended targets *in vivo* [28].

Triclosan, the parent compound from which PT119 is derived, is an antibacterial agent that has been used worldwide in medical and consumer products for more than 20 years [29,30]. However, despite the almost ubiquitous occurrence of triclosan, pharmacokinetic studies on this compound are sparse [31]. In a previous study of orally ingested triclosan in humans, the drug appears to be readily absorbed from the gastrointestinal tract and has a rapid turnover. However the high lipophilicity of the drug gives rise to questions regarding distribution properties and accumulation [32]. We previously reported the pharmacokinetics and *in vivo* efficacy against *Francisella tularensis* of PT04, an analog of PT119 [33]. Like PT04, which successfully cleared infection in an *F. tularensis* murine model [33], PT119 also decreased bacterial load in *S. aureus* murine model (Fig. 4). However, to our knowledge the present study is the first to analyze the tissue distribution of a triclosan derivative. The antibacterial efficacy of the saFabI inhibitor AFN-1252 (Affinium Pharmaceuticals, Toronto, ON, Canada) is reported to be driven by AUC/MIC rather than Time > MIC [34], and thus we would expect the same PD parameter to predict PT119 efficacy because both compounds have similar modes of action. In this regard, it is interesting to note that the AUC/MIC value for PT119 at 40 m/kg is only 3.5 despite the fact that this dose of PT119 reduces CFUs by 2 logs in the thigh infection model (AUC/MIC value for AFN-1252 at 30 mg/kg is 20 [34]). Since the PET studies suggest that PT119 has similar blood and tissue concentrations, we speculate that the *in vivo* efficacy of this compound results partly from the long half time of the saFabI:PT119 drug-target complex ($t_R$ 750 min).

We initially speculated that [$^{11}$C]PT119 would accumulate in infected tissue to a higher concentration than that in healthy tissue, given the ability of this compound to decrease bacterial burden coupled with the long residence time of the compound on the enzyme target. However, *ex vivo* analysis revealed that the concentration of [$^{11}$C]PT119 in the thigh was unaffected by infection. Although further studies are required to definitively explain why infection did not change the apparent biodistribution of [$^{11}$C]PT119, it may simply be that the accumulation of drug in the bacteria was insufficient relative to the background signal to differentiate the change in PT119 concentration caused by bacterial infectoion. In addition, we are aware that substituted diphenyl ethers such as PT119, are subject to both Phase I and Phase II metabolism, including O-glucuronidation [33]. Thus, only a portion of the detected signal may arise from the pharmacologically active agent,

Please cite this article in press as: H. Wang, et al., Radiosynthesis and biological evaluation of a novel enoyl-ACP reductase inhibitor for *Staphylococcus aureus*, European Journal of Medicinal Chemistry (2014), http://dx.doi.org/10.1016/j.ejmech.2014.09.008

**Table 2**
Biodistribution in the systemic infection model.

| | Spleen | Lung | Liver | Kidney | Blood |
|---|---|---|---|---|---|
| *Healthy control* | | | | | |
| 20 min | 0.67 ± 0.12 | 3.19 ± 0.13 | 11.79 ± 1.09 | 2.22 ± 0.19 | 0.64 ± 0.08 |
| 40 min | 0.37 ± 0.03 | 1.75 ± 0.13 | 9.69 ± 1.40 | 1.41 ± 0.09 | 0.41 ± 0.07 |
| 60 min | 0.19 ± 0.01 | 1.32 ± 0.13 | 6.91 ± 1.60 | 0.93 ± 0.06 | 0.34 ± 0.03 |
| *Systemic infected* | | | | | |
| 20 min | 0.71 ± 0.05 | 3.28 ± 0.31 | 11.18 ± 0.89 | 2.41 ± 0.08 | 0.67 ± 0.09 |
| 40 min | 0.30 ± 0.10 | 1.78 ± 0.69 | 5.25 ± 1.69 | 1.15 ± 0.14 | 0.38 ± 0.14 |
| 60 min | 0.31 ± 0.03 | 2.01 ± 0.08 | 7.31 ± 1.76 | 1.13 ± 0.07 | 0.44 ± 0.01 |

Values given are [%ID/cc].

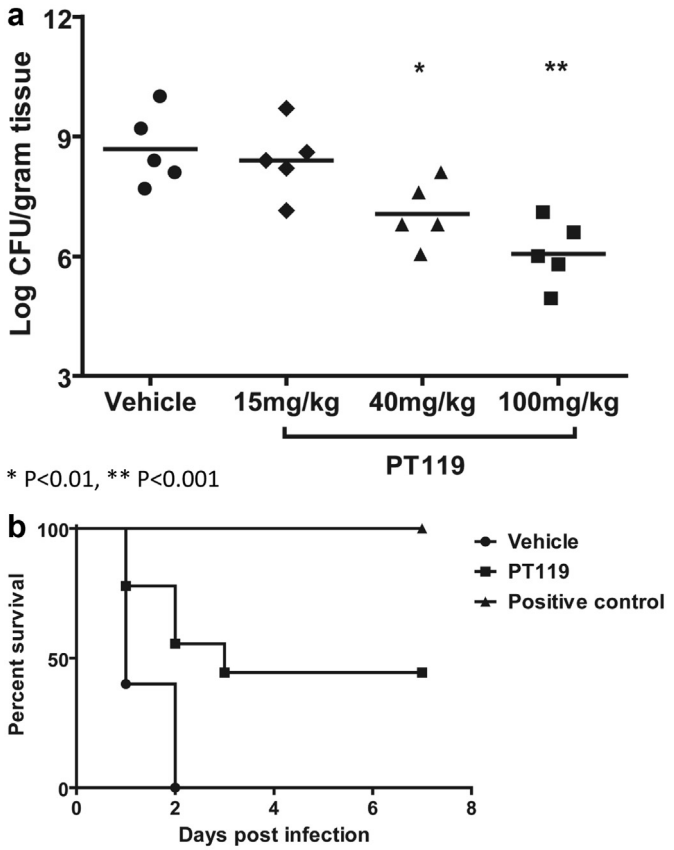


**Fig. 4.** *In vivo* efficacy of PT119. a. *In vivo* efficacy in thigh infection model. Bacterial burden in the infected thighs 24 h post-treatment with a single dose of 15, 40, 100 mg/kg PT119 delivered sc or given vehicle. Bars indicate means of biological replicates. b. *In vivo* efficacy in systemic infected model. Survival plots for *S. aureus* infected mice treated with 100 mg/kg PT119 delivered sc once a day for 3 days following infection and observed until day 7.

again limiting our ability to detect changes in concentration due to bacterial accumulation. Finally, the observation window permitted by the short half life of carbon-11 may be insufficient to fully capture the tissue distribution of the drug. To address these possibilities, on going studies are focused on the introduction of fluorine-18 into saFabI inhibitors that have altered residence times as well as PK and PD properties in order to fully explore the effect of infection on drug biodistribution.

A more detailed understanding of the relationship between pharmacokinetics of antimicrobial drugs and their action on target pathogens (pharmacodynamics) has led to greater sophistication in design of dosage schedules which improves the activity and reduce the selection pressure for resistance in antimicrobial therapy. This, in turn, may be informative in the pharmaceutical development of antimicrobial drugs [35]. Like most antibacterial agents, PT119 requires transport to the site of infection and interaction with the pathogen. As a result, determining the drug concentration at the site of action is a more accurate approach to determining pharmacodynamic relationships than plasma drug concentration [36]. This study presents a promising model to evaluate pharmacokinetics/pharmacodynamics relationships based on target tissue concentrations.

It has been reported that [$^{18}$F]FDG accumulated in *S. aureus* infected thigh muscles to a level 2.3–2.6 times greater than in the healthy thigh [37]. However, [$^{18}$F]FDG is a non-specific marker of glycolytic activity that relies upon a host inflammatory response and cannot discriminate sterile inflammation from infection [38]. By targeting intracellular pathogen enzymes rather than the inflammatory response of the host, radiolabelled drugs especially those with significant drug-target lifetime and quick clearance, are promising candidates for probes to detect and localize bacteria. We have previously demonstrated that PT119 has a significant residence time of 750 min on saFabI [19]. Since the half-life of $^{11}$C is only 20.4 min, using a longer-lived PET isotope, such as $^{18}$F (half-life 109.8 min) or $^{124}$I (half-life 4.2 days), could potentially be used to achieve the goal though this would be a different drug molecule and the similarity in their properties would need to be determined. In addition, increasing the interval between tracer administration and imaging could further increase signal-to-background ratio by allowing the washout of the background PET signal in future investigation.

## 5. Conclusions

In summary, a novel time-dependent saFabI inhibitor, PT119, with optimal drug-target interactions, long residence time and promising MIC, has been labeled with the positron emission isotope carbon-11. [$^{11}$C]PT119 was synthesized using one-step cyanation, purified and formulated within 1 h, with >98% radiochemical purity. Synthesis of this compound allows for analysis of the biodistribution of the labeled drug in mice using PET. The studies demonstrated that there is rapid accumulation of drug and/or its labeled metabolites in tissues, but that there is no significant difference in distribution between infected animals and healthy animals during the ~1 h time course of the drug biodistribution following administration. Studies in mice also demonstrated that

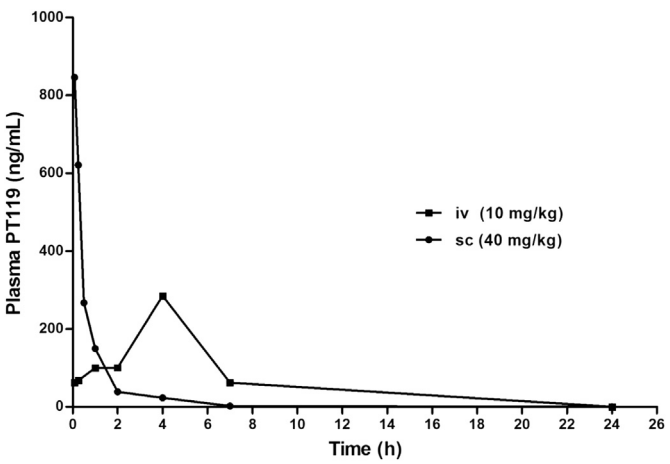


**Fig. 5.** Bioavailability and *in vivo* pharmacokinetics of PT119. Bioavailability was assessed by administering PT119 via iv (10 mg/kg) or sc (40 mg/kg) and determining the amount of compound in blood over 24 h.

Please cite this article in press as: H. Wang, et al., Radiosynthesis and biological evaluation of a novel enoyl-ACP reductase inhibitor for *Staphylococcus aureus*, European Journal of Medicinal Chemistry (2014), http://dx.doi.org/10.1016/j.ejmech.2014.09.008

**Table 3**
*In vivo* pharmacokinetic parameters for PT119 delivered iv and sc.

| Route and dose | iv 10 mg/kg | sc 40 mg/kg |
|---|---|---|
| $V_{ss}$ (mL) | 475.6 | |
| $V_Z$ (mL) | 704.1 | |
| CL(mL/h) | 438.8 | |
| MRT[a] (h) | 0.65 | 6.47 |
| $t_{1/2}$ (h) | 1.01 | 6.17 |
| $C_{max}$ (μg/mL) | 0.84 | 0.28 |
| $T_{max}$ (h) | 0.08 | 4 |
| $AUC_{0-\infty}$ (h*μg/mL) | 0.64 | 1.77 |
| AUC (h*μg/mL)/MIC (μg/mL) | 1.28 | 3.54 |
| Bioavailability F(0, ∞) (%) | | 69 |

[a] MRT, mean residence time.

PT119 was able to decrease bacterial load in both the thigh muscle infection model and systemic infection model. These studies provide an opportunity to review the pharmacokinetics of this new drug in two different *S. aureus* infected mice models which will aid in further optimization of this inhibitor series and will ultimately provide a more accurate approach to determine PK/PDs relationships than plasma drug concentration. These results also indicate that future PET studies in human subjects will yield valuable insights into the clinical application of this drug or other similar drugs, and also set the scene for imaging the distribution of the pathogen *in vivo*.

## Acknowledgement

We are grateful to Dr. Michael Schueller for cyclotron operations, and the PET imaging team at BNL (David Alexoff, Youwen Xu, Colleen Shea and Lisa Muench) for technical assistance.

This work was funded by grants to PJT from NIH (GM102864) and from Stony Brook University (TRO Fusion Award).

## Appendix A. Supplementary data

Supplementary data associated with this article can be found in the online version, at http://dx.doi.org/10.1016/j.ejmech.2014.09.008. These data include MOL file and InChiKey of the most important compounds described in this article.

## References

[1] O. Langer, M. Muller, Methods to assess tissue-specific distribution and metabolism of drugs, Curr. Drug. Metab. 5 (2004) 463–481.
[2] M. Muller, A.D. Pena, H. Derendorf, Issues in pharmacokinetics and pharmacodynamics of anti-infective agents: distribution in tissue, Antimicrob. Agents Chemother. 48 (2004) 1441–1453.
[3] J.G. Pasipanodya, S. Srivastava, T. Gumbo, Meta-analysis of clinical studies supports the pharmacokinetic variability hypothesis for acquired drug resistance and failure of antituberculosis therapy, Clin. Infect. Dis. 55 (2012) 169–177.
[4] J.S. Fowler, N.D. Volkow, G.J. Wang, Y.S. Ding, S.L. Dewey, PET and drug research and development, J. Nucl. Med. 40 (1999) 1154–1163.
[5] A.J. Fischman, N.M. Alpert, J.W. Babich, R.H. Rubin, The role of positron emission tomography in pharmacokinetic analysis, Drug. Metab. Rev. 29 (1997) 923–956.
[6] M.A. Pfaller, R.N. Jones, G.V. Doern, H.S. Sader, K.C. Kugler, M.L. Beach, S.P. Grp, Survey of blood stream infections attributable to gram-positive cocci: frequency of occurrence and antimicrobial susceptibility of isolates collected in 1997 in the United States, Canada, and Latin America from the SENTRY Antimicrobial Surveillance Program, Diagn. Microbiol. Infect. Dis. 33 (1999) 283–297.
[7] D.J. Diekema, M.A. Pfaller, F.J. Schmitz, J. Smayevsky, J. Bell, R.N. Jones, M. Beach, S.P. Grp, Survey of infections due to Staphylococcus species: frequency of occurrence and antimicrobial susceptibility of isolates collected in the United States, Canada, Latin America, Europe, and the Western Pacific region for the SENTRY Antimicrobial Surveillance Program, 1997–1999, Clin. Infect. Dis. 32 (2001) S114–S132.
[8] S.J. Peacock, I. de Silva, F.D. Lowy, What determines nasal carriage of Staphylococcus aureus? Trends Microbiol. 9 (2001) 605–610.
[9] M. Barber, Methicillin-resistant staphylococci, J. Clin. Pathol. 14 (1961) 385–393.
[10] C. Walsh, Microbiology – deconstructing vancomycin, Science 284 (1999) 442–443.
[11] D.M. Sievert, J.T. Rudrik, J.B. Patel, L.C. McDonald, M.J. Wilkins, J.C. Hageman, Vancomycin-resistant staphylococcus aureus in the United States, 2002–2006, Clin. Infect. Dis. 46 (2008) 668–674.
[12] D.J. Payne, W.H. Miller, V. Berry, J. Brosky, W.J. Burgess, E. Chen, W.E. DeWolf Jr., A.P. Fosberry, R. Greenwood, M.S. Head, D.A. Heerding, C.A. Janson, D.D. Jaworski, P.M. Keller, P.J. Manley, T.D. Moore, K.A. Newlander, S. Pearson, B.J. Polizzi, X. Qiu, S.F. Rittenhouse, C. Slater-Radosti, K.L. Salyers, M.A. Seefeld, M.G. Smyth, D.T. Takata, I.N. Uzinskas, K. Vaidya, N.G. Wallis, S.B. Winram, C.C. Yuan, W.F. Huffman, Discovery of a novel and potent class of FabI-directed antibacterial agents, Antimicrob. Agents Chemother. 46 (2002) 3118–3124.
[13] H. Lu, P.J. Tonge, Inhibitors of FabI, an enzyme drug target in the bacterial fatty acid biosynthesis pathway, Acc. Chem. Res. 41 (2008) 11–20.
[14] P.J. Tonge, R. Rawat, A. Whitty, The isoniazid-NAD adduct is a slow, tight-binding inhibitor of InhA, the Mycobacterium tuberculosis enoyl reductase: adduct affinity and drug resistance, Proc. Natl. Acad. Sci. U S A 100 (2003) 13881–13886.
[15] A.I. Bamber, T.J. Neal, An assessment of triclosan susceptibility in methicillin-resistant and methicillin-sensitive Staphylococcus aureus, J. Hosp. Infect. 41 (1999) 107–109.
[16] H.S. Park, Y.M. Yoon, S.J. Jung, C.M. Kim, J.M. Kim, J.H. Kwak, Anti-staphylococcal activities of CG400549, a new bacterial enoyl-acyl carrier protein reductase (FabI) inhibitor, J. Antimicrob. Chemother. 60 (2007) 568–574.
[17] S. Escaich, L. Prouvensier, M. Saccomani, L. Durant, M. Oxoby, V. Gerusz, F. Moreau, V. Vongsouthi, K. Maher, I. Morrissey, C. Soulama-Mouze, The MUT056399 inhibitor of FabI is a new antistaphylococcal compound, Antimicrob. Agents Chemother. 55 (2011) 4692–4697.
[18] B.T. Tsuji, Y. Harigaya, A.J. Lesse, A. Forrest, D. Ngo, Activity of AFN-1252, a novel FabI inhibitor, against Staphylococcus aureus in an in vitro pharmacodynamic model simulating human pharmacokinetics, J. Chemother. 25 (2013) 32–35.
[19] A. Chang, J. Schiebel, W. Yu, G.R. Bommineni, P. Pan, M.V. Baxter, A. Khanna, C.A. Sotriffer, C. Kisker, P.J. Tonge, Rational optimization of drug-target residence time: insights from inhibitor binding to the Staphylococcus aureus FabI enzyme-product complex, Biochemistry 52 (2013) 4217–4228.
[20] H. Lu, K. England, C.A. Ende, J.J. Truglio, S. Luckner, B.G. Reddy, N.L. Marlenee, S.E. Knudson, D.L. Knudson, R.A. Bowen, C. Kisker, R.A. Slayden, P.J. Tonge, Slow-onset inhibition of the FabI enoyl reductase from francisella tularensis: residence time and in vivo activity, ACS Chem. Biol. 4 (2009) 221–231.
[21] D.A. Dohyun Kim, Sung Won Kim, Jacob Hooker, A. Richard, Ferrieri C-11 Cyanide Production System, Brookhaven Science Associates, LLC, 2013.
[22] P. Pan, S.E. Knudson, G.R. Bommineni, H.J. Li, C.T. Lai, N. Liu, M. Garcia-Diaz, C. Simmerling, S.S. Patil, R.A. Slayden, P.J. Tonge, Time-dependent diaryl ether inhibitors of InhA: structure-activity relationship studies of enzyme inhibition, antibacterial activity, and in vivo efficacy, ChemMedChem 9 (4) (2014 Apr) 776–791, http://dx.doi.org/10.1002/cmdc.201300429. Epub 2014 Mar 11.
[23] L. Liu, Y.W. Xu, C. Shea, J.S. Fowler, J.M. Hooker, P.J. Tonge, Radiosynthesis and bioimaging of the tuberculosis chemotherapeutics isoniazid, rifampicin and pyrazinamide in baboons, J. Med. Chem. 53 (2010) 2882–2891.
[24] R.J. Heath, Bacterial fatty-acid biosynthesis: an antibacterial drug target waiting to be exploited, Drug. Discov. Today 6 (2001), 715-715.
[25] C.W. am Ende, S.E. Knudson, N. Liu, J. Childs, T.J. Sullivan, M. Boyne, H. Xu, Y. Gegina, D.L. Knudson, F. Johnson, C.A. Peloquin, R.A. Slayden, P.J. Tonge, Synthesis and in vitro antimycobacterial activity of B-ring modified diaryl ether InhA inhibitors, Bioorg. Med. Chem. Lett. 18 (2008) 3029–3033.
[26] T.J. Sullivan, J.J. Truglio, M.E. Boyne, P. Novichenok, X. Zhang, C.F. Stratton, H.J. Li, T. Kaur, A. Amin, F. Johnson, R.A. Slayden, C. Kisker, P.J. Tonge, High affinity InhA inhibitors with activity against drug-resistant strains of Mycobacterium tuberculosis, ACS Chem. Biol. 1 (2006) 43–53.
[27] R. Nutt, L.J. Vento, M.H.T. Ridinger, In vivo molecular imaging biomarkers: clinical pharmacology's new "PET"? Clin. Pharmacol. Ther. 81 (2007) 792–795.
[28] G.M. Simon, M.J. Niphakis, B.F. Cravatt, Determining target engagement in living systems, Nat. Chem. Biol. 9 (2013) 200–205.
[29] A.M. Calafat, X. Ye, L.Y. Wong, J.A. Reidy, L.L. Needham, Urinary concentrations of triclosan in the U.S. population: 2003–2004, Environ. Health Perspect. 116 (2008) 303–307.
[30] L.Q. Wang, C.N. Falany, M.O. James, Triclosan as a substrate and inhibitor of 3′-phosphoadenosine-5′-phosphosulfate-sulfotransferase and UDP-glucuronosyl transferase in human liver fractions, Drug. Metab. Dispos. 32 (2004) 1162–1169.
[31] C. Queckenberg, J. Meins, B. Wachall, O. Doroshyenko, D. Tomalik-Scharte, B. Bastian, M. Abdel-Tawab, U. Fuhr, Absorption, pharmacokinetics, and safety of triclosan after dermal administration, Antimicrob. Agents Chemother. 54 (2010) 570–572.
[32] G. Sandborgh-Englund, M. Adolfsson-Erici, G. Odham, J. Ekstrand, Pharmacokinetics of triclosan following oral ingestion in humans, J. Toxicol. Environ. Health A 69 (2006) 1861–1873.

[33] K. England, C.A. Ende, H. Lu, T.J. Sullivan, N.L. Marlenee, R.A. Bowen, S.E. Knudson, D.L. Knudson, P.J. Tonge, R.A. Slayden, Substituted diphenyl ethers as a broad-spectrum platform for the development of chemotherapeutics for the treatment of tularaemia, J. Antimicrob. Chemother. 64 (2009) 1052–1061.

[34] M.A. Banevicius, N. Kaplan, B. Hafkin, D.P. Nicolau, Pharmacokinetics, pharmacodynamics and efficacy of novel FabI inhibitor AFN-1252 against MSSA and MRSA in the murine thigh infection model, J. Chemother. 25 (2013) 26–31.

[35] O.A. Mckellar, S.F.S. Bruni, D.G. Jones, Pharmacokinetic/pharmacodynamic relationships of antimicrobial drugs used in veterinary medicine, J. Vet. Pharmacol. Ther. 27 (2004) 503–514.

[36] J. Barre, F. Didey, F. Delion, J.P. Tillement, Problems in therapeutic drug monitoring: free drug level monitoring, Ther. Drug. Monit. 10 (1988) 133–143.

[37] M.M. Welling, R. Alberto, Performance of a (99m)Tc-labelled 1-thio-beta-D-glucose 2,3,4,6-tetra-acetate analogue in the detection of infections and tumours in mice: a comparison with [(18)F]FDG, Nucl. Med. Commun. 31 (2010) 239–248.

[38] A. Signore, A.W. Glaudemans, The molecular imaging approach to image infections and inflammation by nuclear medicine techniques, Ann. Nucl. Med. 25 (2011) 681–700.

Please cite this article in press as: H. Wang, et al., Radiosynthesis and biological evaluation of a novel enoyl-ACP reductase inhibitor for *Staphylococcus aureus*, European Journal of Medicinal Chemistry (2014), http://dx.doi.org/10.1016/j.ejmech.2014.09.008